Experiments in Fluids 9, 222–230 (1990)

Experiments in Fluids

Measurements of turbulent flow in a channel at low Reynolds numbers

M. A. Niederschulte, R. J. Adrian and **T. J. Hanratty**

University of Illinois, Urbana, IL 61801, USA

Abstract. Normal and streamwise components of the velocity fields of turbulent flow in a channel at low Reynolds numbers have been measured with laser-Doppler techniques. The experiments duplicate the conditions used in current direct numerical simulations of channel flow, and good, but not exact, agreement is found for single-point moments through fourth order. In order to eliminate LDV velocity bias and to measure velocity spectra, the mean time interval between LDV signals was adjusted to be much smaller than the smallest turbulence time scale. Spectra of the streamwise and normal components of velocity at locations spanning the channel are presented.

1 Introduction

This paper presents measurements, made with a two-component laser-Doppler velocimeter, of the streamwise and normal velocity fields for turbulent flow in a rectangular channel. They were obtained at low velocites, so that the Reynolds number, based on the half channel height and the bulk velocity, was 2,777 or 2,457, and the dimensionless half width of the channel was $H^+ = 178.6$ or $H^+ = 158.5$, respectively. The motivation for this work was to examine the accuracy of the direct numerical simulation of three dimensional, time dependent turbulent flow in a channel at $Re_B = 2{,}800$ by Kim et al. (1987) and to obtain new measurements of the power spectral densities of both streamwise and normal turbulent velocity components.

The study reported in this paper is part of a Ph.D. thesis by M. Niederschulte (1989). Measurements were made in fully developed flow 200 channel heights downstream from the entrance of a 5.08×61 cm rectangular channel by using a two-component laser Doppler velocimeter. Certain aspects of the LDV and the experimental procedure were tailored to the demands of this flow and make this experiment unique. Firstly, the optics were designed to permit accurate measurements at distances as close to the wall as $y^+ = 0.6$ (0.16 mm) with spatial resolution better than 0.035 mm in the direction normal to the wall. This was accomplished by using a three-beam LDV of the type described by Adrian (1975), combined with 6.27:1 expansion of the laser beams, as described in Buckles et al. (1984). Secondly, the fluid and the scattering medium in the fluid were also managed carefully to avoid the uncertainties associated with LDV velocity bias, and to produce data whose rate was large enough to permit measurement of the power spectra of the relatively low turbulence intensity flow. Carefully cleaned water was seeded with 808 nm polystyrene particles having a specific gravity of 1.05 and standard distribution of 0.5%. The concentration of this very uniform scattering medium was chosen, in accord with the discussion in Adrian (1983), to be large enough to yield time intervals between particle arrivals that were smaller than the smallest turbulence time scale, but not so small as to create ambiguity (or "phase") noise. On average, the mean separation between particles in the streamwise direction was less than 0.2 mm. The resulting signal was a nearly continuous representation of the velocity time history.

Measurements were obtained of the mean velocity, the Reynolds stress, the mean-square of the streamwise and normal velocity components, and the skewness and flatness of the fluctuating velocity components. The comparison with the direct numerical simulation is encouraging. The very close agreement between the measurements of the mean-square of the normal velocity fluctuations, $\overline{v^2}$, and the simulation removes the problems that existed in a previous comparison (Kim et al. 1987) with hot-wire or hot-film measurements. The small, but significant, differences noted with the streamwise velocity fluctuations suggest that more nodes or a larger computational domain in the flow direction would slightly improve the computation.

Because the time interval between bursts was small compared to the smallest time scale of the turbulence the filtered signals from the trackers could be analyzed to obtain the spectral functions of the streamwise and normal velocity fluctuations. These two spectral functions are compared and the influence of wall distance is examined.

2 Experiments

The research was carried out in a flow loop that circulated water through a rectangular channel at a controlled temper-

ature and that was specially designed for optical experiments (Niederschulte 1989). The flow channel is preceded by a nozzle which changes from a 59.9 cm × 76.2 cm cross-section to a 5.08 cm × 61 cm cross-section. A 15.2 cm long honeycomb with 2.54 cm square cells is located at the inlet to the nozzle. A boundary-layer trip is located at the outlet just before the 5.08 cm × 61 cm channel to decrease the length of channel needed to obtain a fully developed flow. It is a plate with a rectangular hole slightly smaller than the cross-section of the channel so that it extends 0.254 cm into the flow from all four walls. The channel preceding the test section is constructed from stainless steel and has a total length of 711 cm. It has a deviation from the specified dimensions of less than 0.005 and the 305 cm long test section deviates by less than 0.0005 cm.

The channel was filled with de-ionized water which was cleaned with 3 μm filters. Algae growth was avoided by adding Chlorox and by excluding access of light to the system. Dissolved air was removed from the water through bleed lines by heating slightly and pulling a vacuum. The polystyrene particles used for seeding were made by procedures outlined by Juarg and Krieger (1976) and by Goodwin et al. (1978). Two different sizes were explored, 568 nm and 808 nm. A scanning electron photograph showed the particles to be spherical and to have a standard deviation of 0.5%. The 808 nm particles were chosen for the experiments. They gave a stronger signal, yet did not increase the opacity of the liquid to unacceptable levels. The quantity of particles added was such that a burst density, defined as the mean number of particles in the measuring volume (Adrian 1983), was approximately 0.2.

The LDV system was constructed from standard TSI, Inc. components. It used a three beam configuration, with separation by cross-polarization, to measure the u-(streamwise) and v-(normal) components of velocity. Beams 1 and 2 measured the $u+v$ component directly, and beams 2 and 3 measured the $u-v$ component directly. The u- and v-components were found by summing and differencing the measurements. The beams entered the channel through an optical window, polished to a surface flatness of $\lambda/10$, on the 50.8 mm side and scattered light was collected through an identical window on the other 50.8 mm side.

In order to place the measuring volume as close as 0.12 mm from the surface without blocking the two lower beams the transmitting optics were tilted 0.7° towards the surface. The receiving optics were tilted upward by about 2° to reduce the light reflected from the surface. The receiving optics were also rotated slightly to the side of the optical axis to prevent reception of flare and intense reflected light from the surface of the channel. All of the optics were mounted on a three dimensional translation table whose vertical and streamwise movements could be monitored to within 0.025 mm.

A small measurement volume was formed from the standard TSI optics by using two 2.27 : 1 beam expanders ahead of a 250 mm focal length lens. In combination with the 1.1 : 1 expansion introduced by the laser beam collimator the total expansion ratio was 6.27 : 1. The dimensions of the measuring volume were calculated to be $d_m = 35$ μm and $l_m = 300$ μm.

The receiving optics collected and separated the scattered light into two perpendicular polarity components which were focused onto 0.2 mm pinholes in front of separate photomultipliers. Frequency shifting at approximately twice the mean Doppler frequency was used to obtain a Doppler signal in the range where the signal processors worked best, and to increase the apparent number of fringes to approximately 18 per Doppler burst.

The signals from the two photomultipliers were downmixed, high-pass filtered at the shift frequency to remove the pedestals, low-pass filtered to remove high frequency noise, and processed by TSI model 1090 frequency trackers. The analog outputs of the trackers sampled the frequency of each Doppler burst and held that value until a new sample arrived. According to the analysis of Adrian and Yao (1987), the power spectrum of the sampled-and-held velocity consists of a white "step-noise" component plus the true spectrum of the velocity, each of these being low-pass filtered by the effect of missing information during the hold periods. The cut-off frequency of this filter is equal to the mean data rate over 2π. At the centerline of the channel, where the velocity was approximately 11 cms^{-1}, the mean data rate was approximately 2,500 samples per second. Hence, the low pass cut-off due to holding the signal occurred around 400 Hz. (The exceptionally high data rate was a consequence of the care taken in seeding the flow. For comparison, the equivalent data rate in a 11 ms^{-1} flow with unexpanded laser beams would be 10^6 samples per second.) The analog outputs were low-pass filtered at 100 Hz to remove high frequency energy associated with the steps in the sampled and held signal, and the filtered signal was digitized at 100 Hz. This frequency was sufficient, since all of the turbulent energy lay below 50 Hz, which was also much less than the low pass cut-off due to the hold periods. Thus, accurate, undistorted spectra were measured. The sample size was 40,960 points.

3 Corrections for noise and dropout

The output voltages from the two trackers contained noise and dropout. The noise consisted of small errors in the measurement of each individual Doppler burst plus step noise. Drop-outs occurred when the trackers were unable to stay locked onto the LDV signal.

A moving window that followed the instantaneous voltage fluctuations was used in the computer program to correct for large excursions due to dropout. Voltage values outside of this window were considered to be unphysical and were removed. The window was set equal to the time-averaged voltage ± 2.75 times the standard deviation of the data covered by the window. The time resolution of the signal was

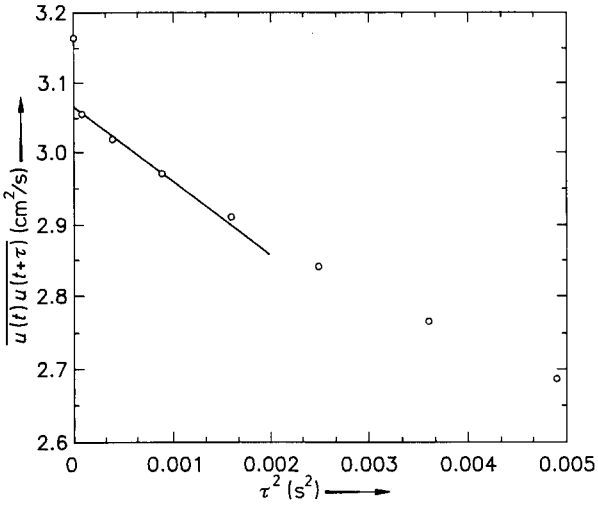

Fig. 1. Auto-correlation plotted versus the square of the time delay

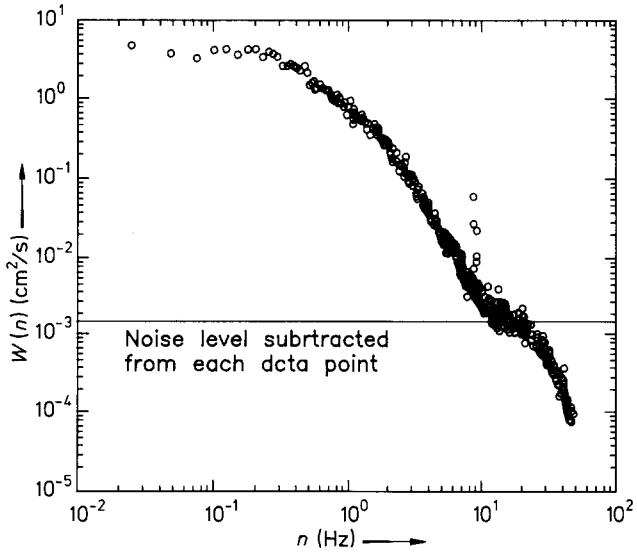

Fig. 2. Uncorrected streamwise spectra at $y u^+/\nu = 16.4$, $Re = 2{,}777$; the horizontal line shows the noise plateau which will be subtracted from the data

fine enough that the fluid velocity (and therefore the voltage) could not change by more than 2.75 standard deviations in one time increment.

The window length was set at 1/5 of the number of points sampled in one second. This length was chosen as a compromise between a time long enough to insure that dropout data would not strongly influence the calculation of the size of the window and a time short enough to permit the window to follow accurately the voltage fluctuations. The number of points removed was under 5% of the total.

A noise correction for the intensities and the Reynolds stress was made by recognizing that the noise was correlated only for very small times. A plot of the time delayed auto correlation of u, Fig. 1, indicates a sharp increase in the correlation at $\tau = 0$. Since the velocity auto-correlation should vary as τ^2 for $\tau \to 0$ this increase is interpreted as being due to wide-ban noise. The noise power could be calculated by subtracting the extrapolation of the intercept of the $\overline{u(t)\,u(t+\tau)}$ versus τ^2 curve from the measured $\overline{u^2}$ at $\tau = 0$.

The correction for the spectral measurements was made by assuming the noise was white, that is, the spectral density function is flat over the frequency range considered. This was supported by spectra determined from the raw measurements. An example is given in Fig. 2. The drop-off at large frequencies was determined by the low-pass filter operating on the analog output of the frequency tracker. If a larger cut-off frequency was used than was the case for the data in Fig. 2 the plateau indicated by the straight line would have extended to higher frequencies. This plateau defined the spectral density function of the white noise which was subtracted from the measurements to obtain velocity spectra. The cut-off frequency of this filter was, therefore, a compromise in that it was chosen to be large enough to determine the noise correction, yet not so large that too much of the noise signal was included in the calculation of the spectral function. The total amount of noise calculated in this manner agreed closely with noise calculated from measurements of the Eulerian correlation coefficient.

4 Experimental conditions

The conditions for the experiments are listed in Table 1. Separate runs were made at $Re = 2{,}776$ and at $Re = 2{,}778$. The run at $Re = 2{,}778$ measured the velocity field from the bottom wall to the channel center and the run at $Re = 2{,}776$ made measurements from the top wall to the channel center. The experiments at $Re = 2{,}457$ were done so as to make direct comparisons with the results of a direct numerical simulation of channel flow by Lyons (1989).

5 Comparison of velocity measurements and the computer simulation

Velocity measurements were made non-dimensional with the friction velocity, u^*, and distances with the viscous length, ν/u^*. The friction velocity was determined from the total stress measurements

$$\frac{\tau}{\varrho} = -\overline{uv} + \nu \frac{d\bar{U}}{dy}. \tag{1}$$

These are shown in Fig. 3 wherein u^* is picked so that the dimensionless total stress equals $+1$ at the bottom wall and -1 at the top wall. Values of the wall stress calculated in this way were the same as values obtained from the slope of $\bar{U}(y)$ for $y \to 0$; i.e.,

$$\tau_w = \mu \left(\frac{d\bar{U}}{dy}\right)_{y=0}. \tag{2}$$

Measurements of time-averaged velocity are plotted in Fig. 4. A logarithmic coordinate is used for the dimension-

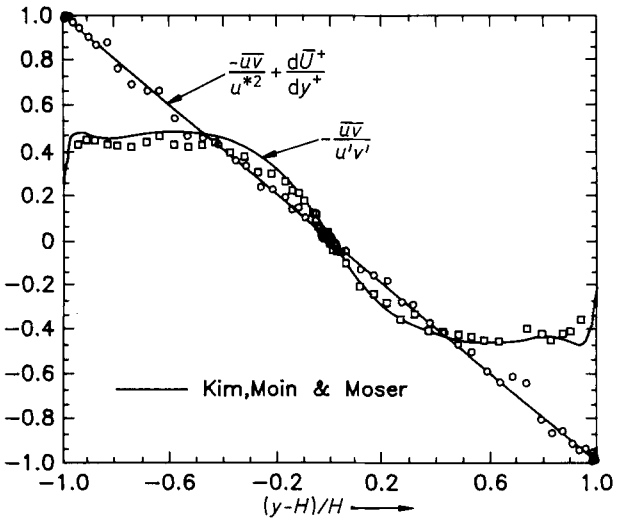

Fig. 3. Dimensionless total stress and the Reynolds stress correlation at $Re = 2{,}777$

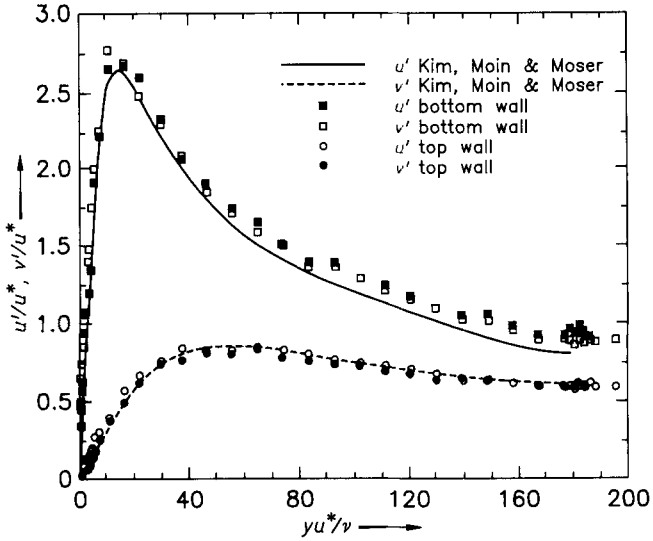

Fig. 5. Root-mean-square of the fluctuations in the streamwise, $u' = (\overline{u^2})^{1/2}$, and normal, $v' = (\overline{v^2})^{1/2}$, velocities

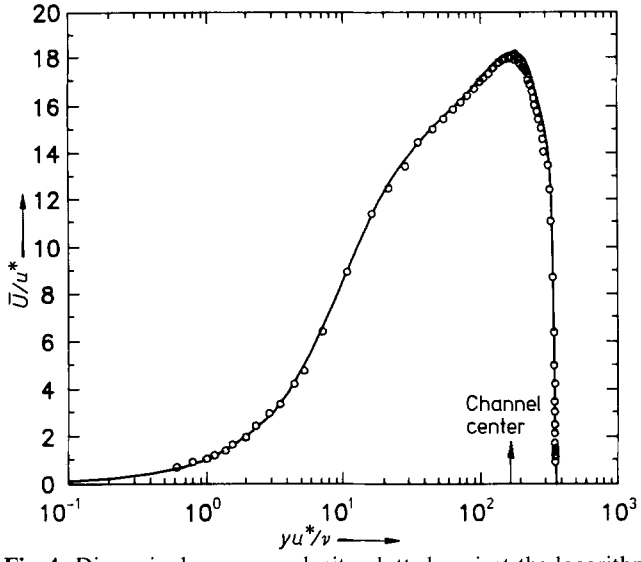

Fig. 4. Dimensionless mean velocity plotted against the logarithm of the distance from the wall at $Re = 2{,}777$

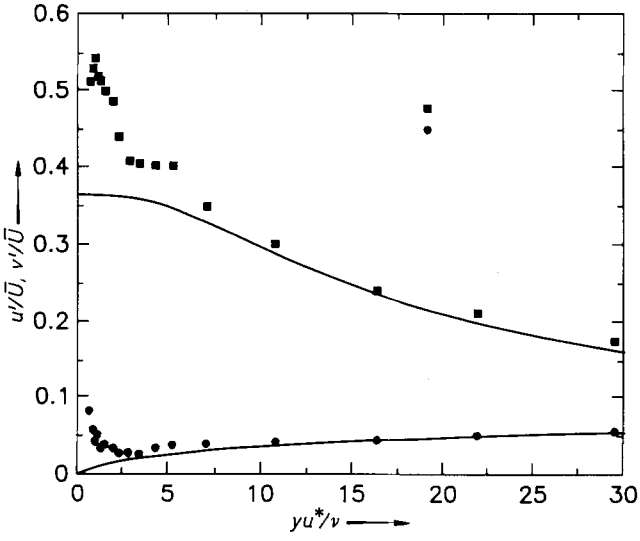

Fig. 6. Root-mean-square velocity; fluctuations made dimensionless with the local mean velocity

less distance from the bottom wall, so the profile appears asymmetric around the center of the channel, $y^+ = 180$. The solid curve represents the computer simulation of Kim et al. (1987). It is noted that twelve points were obtained for $y^+ \leq 5$. These agree with the equation for the viscous sublayer, $U^+ = y^+$.

Good agreement exists between the computation and the experiments. A maximum discrepancy of about 1.4% is noted in the central part of the channel. It should be noted that the simulation produced a slightly asymmetric profile. As a consequence, the differences are greater in the region closer to the top wall.

The measured velocity of the fluid at the center of the channel was 11.8 cm/s. A bulk velocity,

$$U_B = 1/2 \int_{-1}^{1} U \, d\left(\frac{y}{H}\right) \tag{3}$$

normalized with the friction velocity is calculated to be 15.55, in good agreement with the value of 15.63 obtained from the computer simulation. The ratio of the centerline and bulk velocities is 1.16, in exact agreement with the computer calculation.

Measurements of the root-mean-square values of the streamwise, $u' = (\overline{u^2})^{1/2}$, and the normal, $v' = (\overline{v^2})^{1/2}$, velocity fluctuations are given in Fig. 5. Excellent agreement is noted between the computed and measured v'. The measured u' are found to be slightly larger than the computed u'. The difference is outside the range of experimental error and, therefore, of significance.

Measurements of u' and v' in the near wall region are plotted as u'/U and as v'/U in Fig. 6, where U is the local time-averaged velocity. The noise correction for v', discussed in Sect. 3, became larger than the signal close to the wall. Therefore, it is believed that the v' measurements for $y^+ < 3.6$

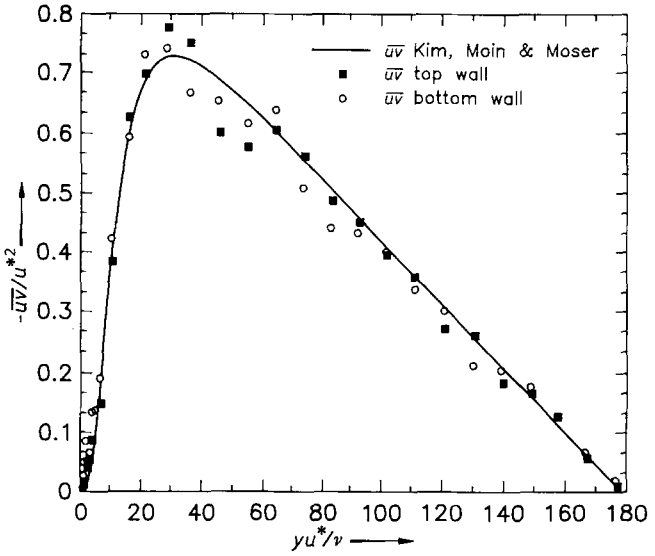

Fig. 7. Dimensionless Reynolds stresses plotted as a function of the dimensionless distance from the wall

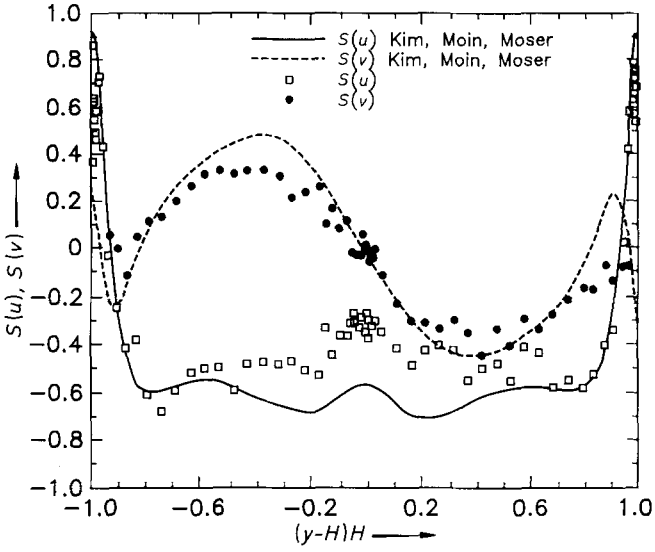

Fig. 8. The skewness factors, $\overline{u_i^3}/(\overline{u_i^2})^{3/2}$, of the streamwise and normal velocity fluctuations

should be disregarded. Excellent agreement between the computer simulation and measurements is noted, if this is taken into account. The measured values of u'/U agree with the computer simulation for $y^+ > 7$. For $2.5 < y^+ < 7$ the measured u'/U are slightly larger than the computer results. However, for $y^+ < 2.5$ the measured u'/U are found to increase dramatically, reaching a maximum of 0.54 at $y^+ = 1$. There is no reason to disregard these points because of an excessive noise-to-signal ratio (as was the case for v'/U at small y^+). It is believed that this maximum is associated with non-turbulent flow oscillations caused by high frequency pressure pulsations in the flow loop. Measurements of the frequency spectrum of the streamwise fluctuations gave no evidence for extraneous flow oscillations at $y^+ = 3.4$. Unfortunately, no spectra were determined for $y^+ < 3.4$. Consequently, the possibility that the sharp peak at $y^+ = 1$ represents real turbulent behavior cannot be ruled out.

Excellent agreement is observed between the measured and computed Reynolds stresses, as shown in Fig. 7. The measurements for $y^+ < 10$ had considerable noise. This was evidenced by erratic results. Consequently, large values of the measured Reynolds stress (compared to the computed values) at small y^+ result from experimental error. Measurements of the Reynolds stress coefficient are plotted in Fig. 3. These are uniformly lower than the computed values, because of the differences in u' shown in Fig. 5.

Skewness and flatness factors, defined as $S = \overline{u_i^3}/(\overline{u_i^2})^{3/2}$ and $F = \overline{u_i^4}/(\overline{u_i^2})^2$, were calculated from the data sets that consisted of 40,960 measured points per velocity component, sampled over a 6.8 min time span.

Figure 8 presents the measured skewness of the streamwise and normal velocity fluctuations. The measured and calculated skewnesses of the streamwise velocity have the same general shape. They agree numerically at distances from the wall of less than 0.5 H. The measurements are smaller at the center region of the channel, in part because the measured u' (which appears in the denominator of the skewness factor) is larger. The magnitudes of the measured maximum and minimum of the skewness of the normal velocity component which occur at $y/H = \pm 0.4$ are slightly smaller than the calculations. Also the measured skewnesses of the normal velocity fluctuations do not show the sharp maximum and minimum at $y/H = \pm 0.9$ indicated by the computer simulations.

Measurements of the flatness factors for the streamwise, $F(u)$, and the normal velocity components, $F(v)$, are given in Fig. 9. Excellent agreement between the measured and computed $F(u)$ is observed. However, the measured $F(v)$, in contrast to the computed $F(v)$, show an almost constant value across the whole channel. In particular, they do not show the rapid increase close to the wall indicated by the computations.

Measurements of the skewness and flatness of uv defined as $S = (\overline{uv})^3/[(\overline{uv})^2]^{3/2}$, $F = (\overline{uv})^4/[(\overline{uv})^2]^2$, shown in Fig. 10, are in fair agreement with the computer simulation.

5 Velocity spectra

Spectral density functions for the streamwise, $W_u(n)$, and the normal, $W_v(n)$, velocity fluctuations are defined as

$$\overline{u^2} = \int_0^\infty W_u(n)\, dn\,, \tag{4}$$

$$\overline{v^2} = \int_0^\infty W_v(n)\, dn\,, \tag{5}$$

where n is the frequency in Hertz. Measurements of $W_u(n)$ and $W_v(n)$ are presented for two conditions: $Re = 2{,}777$ and

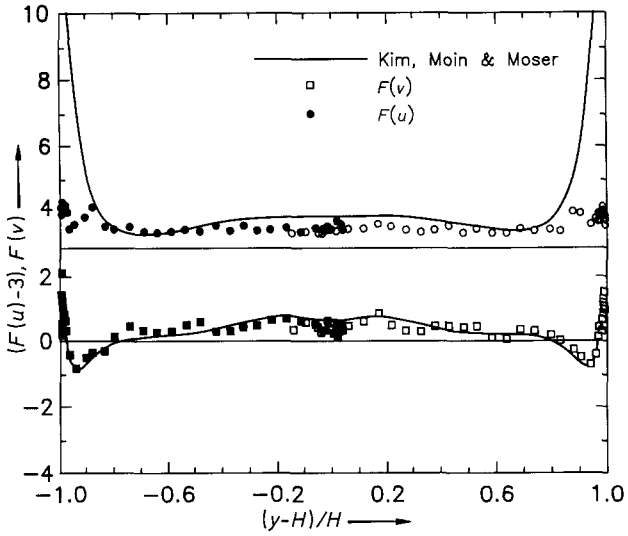

Fig. 9. The flatness factors, $\overline{u_i^4}/(\overline{u_i^2})^2$, of the streamwise and normal velocity fluctuations; the solid horizontal lines are the values for a Gaussian signal

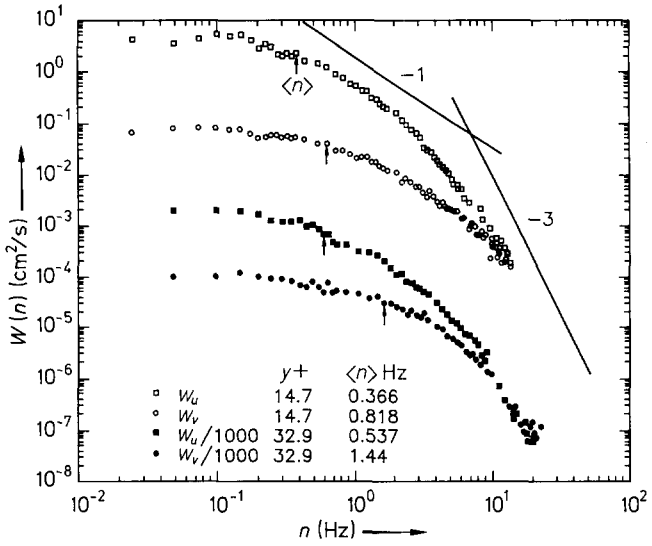

Fig. 11. Spectra of the streamwise and normal velocity components for $y^+ = 14.7$, 32.9 at $Re = 2{,}457$

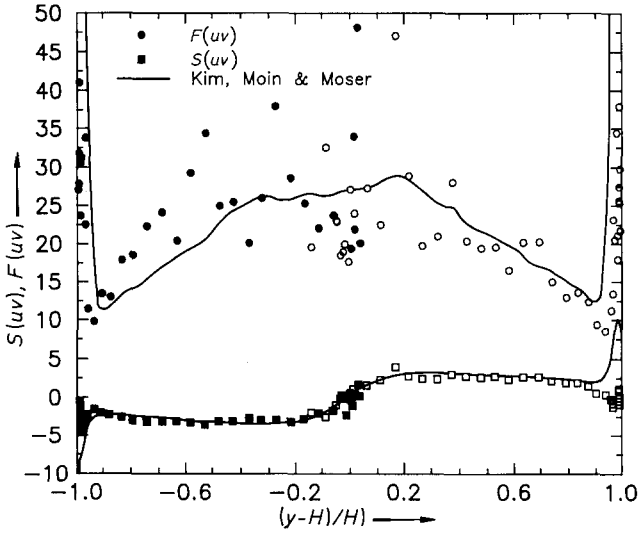

Fig. 10. The skewness and flatness factors for $u\,v$

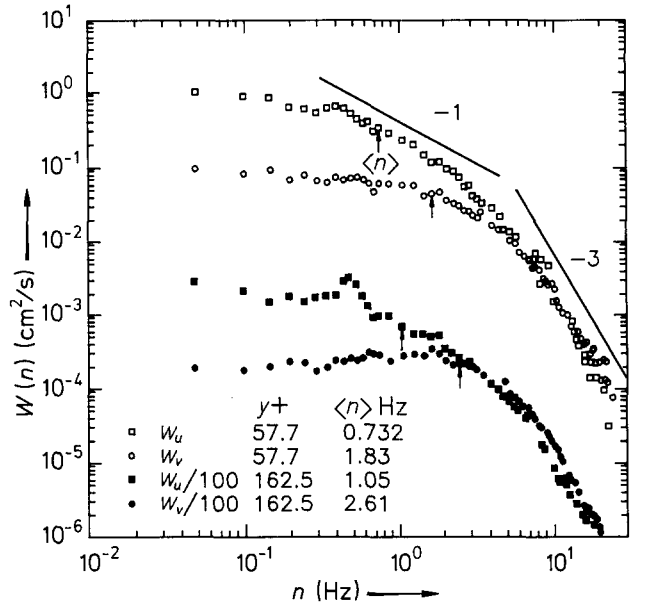

Fig. 12. Spectra of the streamwise and normal velocity components for $y^+ = 57.7$, 162.5 at $Re = 2{,}457$

$Re = 2{,}457$ (Table 1). Most of the discussion will center on the measurements at $Re = 2{,}457$, since these present a more consistent picture.

Figures 11 and 12 show spectral measurements for $Re = 2{,}457$ at $y^+ = 14.7$, 32.9, 57.7, 162.5. The median frequency, below which half of the energy is contained, is indicated by the arrow and designated in the caption. It is noted that the range of frequencies is about the same for all y^+. A striking feature is that the spectral density functions for the streamwise and normal velocity fluctuations are approximately the same at high frequencies. There appears to be a range of frequencies where the spectral function for the streamwise fluctuations varies approximately as n^{-3}.

Figure 13 shows the effect of increasing distance from the wall on the spectral density function for the streamwise velocity fluctuations. The median frequencies, $\langle n \rangle$, are listed for the spectra at each y^+. It is noted that the increase in $\overline{u^2}$ from $y^+ = 2.7$ to $y^+ = 14.7$ is accommodated by an increase in the energy content of all frequencies. The spectral density function is roughly the same at high frequencies for $y^+ = 32.9$, 57.7, 162.5. The decrease in $\overline{u^2}$ with increasing y^+ outside the viscous wall layer is associated with a decrease in the energy of medium and low frequency eddies.

The effect of distance from the wall on the spectral density function for the normal velocity fluctuations is shown in Fig. 14. The increase in $\overline{v^2}$ from $y^+ = 2.7$ to $y^+ = 14.7$ is ac-

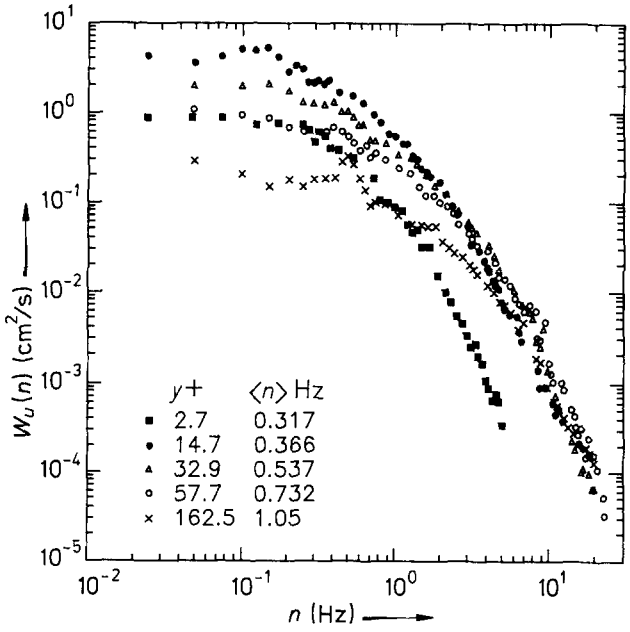

Fig. 13. Spectra of the streamwise velocity component at $Re = 2{,}457$

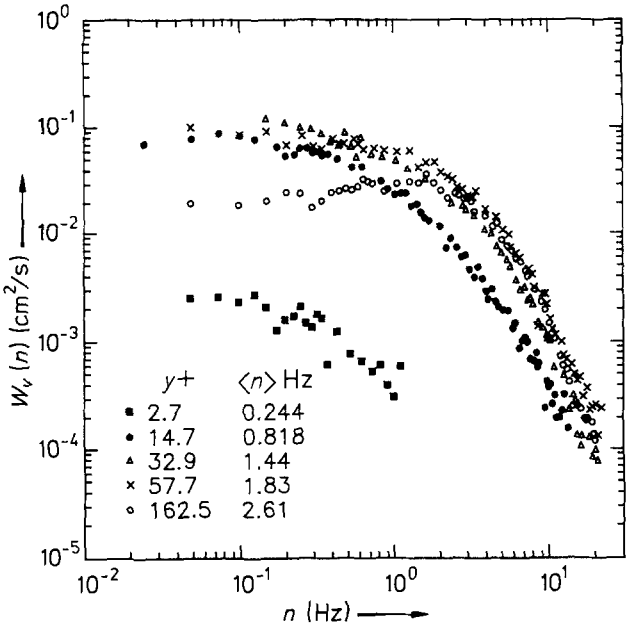

Fig. 14. Spectra of the normal velocity component at $Re = 2.457$

Table 1. Run conditions for velocity data sets

Reynolds no.	2,457	2,778	2,776
Bulk velocity (cm/s)	8.998	10.172	10.167
Half channel height (H^+)	158.5	178.5	178.7
Volumetric flowrate (l/s)	2.675	3.024	3.023
Kinematic viscosity (cS)	0.008930	0.008930	0.008930
Friction velocity (cm/sec)	0.5805	0.6537	0.6545
Friction factor	0.008324	0.008260	0.008287
Distance of $y^+ = 1$ (mm)	0.1538	0.1366	0.1364
Diameter of m.v. (plus units)	0.2275	0.2562	0.2565
Length of m.v. (plus units)	1.6251	1.8301	1.8323
Wall location of data set	Bottom	Bottom	Top

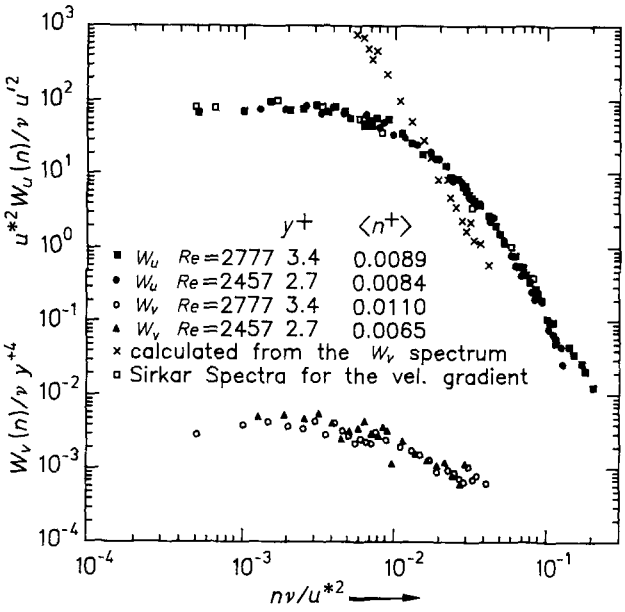

Fig. 15. Spectra of the streamwise velocity fluctuations in the viscous sub-layer

companied by an increase of the energy content of eddies of all frequencies. The spectral functions for $y^+ = 32.9$, 57.7, 162.5 are roughly the same for high frequencies. The normal intensities, $\overline{v^2}$, for $y^+ = 32.9$ and 57.7 are roughly the same, as are the spectral density functions. The small decrease in $\overline{v^2}$ from $y^+ = 57.7$ to $y^+ = 162.5$ is associated mainly with a decrease in the energy content of the low frequency eddies (and not the energy containing eddies).

Spectral density functions for the streamwise and normal velocity fluctuations in the viscous sub-layer are shown in Fig. 15. It is noted that the normalization of the measured $W_v(n)$ with y^{+4} (since $\overline{v^2} \sim y^{+4}$ in the viscous sub-layer) brings into agreement spectra measured at $y^+ = 2.7$ and 3.4. The range of frequencies covered at these small y^+ was limited by noise.

Similarity is also indicated in $W_u(n)$. Spectral density measurements normalized with y^{+2} (since $\overline{u^2} \cong (0.36)^2 y^{+2}$ in the viscous sub-layer) agree for $y^+ = 2.7$ and $y^+ = 3.4$. Good agreement is also noted with the measurement of the spectral density function of fluctuations in streamwise component of the velocity gradient at the wall, obtained by Sirkar (Hanratty et al. 1977).

6 Discussion

6.1 Velocity moments

The overriding conclusion is that the good agreement between laboratory measurements and the direct numerical simulations provide support for the accuracy of time dependent, three-dimensional computer codes developed for turbulent flow in a channel at low Reynolds numbers. Nevertheless, some of the differences should be discussed.

The present measurements suggest that the direct numerical simulation of Kim et al. (1987) is under-estimating the streamwise velocity fluctuations by a small amount. One explanation for this is that the mesh size in the flow direction is not fine enough or that the periodicity length is not large enough. Some support for this can be obtained from the computer experiments of Lyons (1989). These were conducted at $Re = 2{,}200$, $H^+ = 150$. They used 65 Chebyshev polynomials in the y-direction, 128 Fourier components in the z-direction and 32, 64, 128 Fourier components in the x-direction. The computed v' profiles were not sensitive to the resolution in the flow direction, and are in good agreement with LDV measurements of Niederschulte (1989) at $Re = 2{,}457$. However computed u' profiles were lower than the measurements but improved as the number of Fourier components in the x-direction increased. It was also found that the computer simulation tended to under predict the mean velocities but that this difference became quite small as the resolution in the flow direction improved.

Some differences from the computer simulation are noted in measurements of skewness and flatness factors. The computed S_u have slightly larger negative values in the center half but are in good agreement with measurements over the remainder of the channel. This disagreement could be related to the disagreement in $\overline{u^2}$ since the skewness has the term $(\overline{u^2})^{3/2}$ in the denominator. However, this explanation seems to be contradicted by the good agreement of the measured and computed F_u.

More significant differences are noted for the flatness and skewness of the normal velocity fluctuations. The measured S_v and F_v show the same trend as the computations, but are slightly lower, over most of the channel. However, the measurements do not support the large computed changes in S_v and F_v for $y^+ < 30$. In fact, the measurements indicate that the probability distribution of v-fluctuations is close to Gaussian in this region.

6.2 *Spectral density functions*

This investigation showed how careful attention to particle seeding and to the elimination of noise allows for LDV measurements of spectra.

The measurements of the spectral function of the fluctuations of the streamwise component of the velocity gradient at the wall by Sirkar, shown in Fig. 15, were obtained with flush mounted electrochemical probes. These experiments were performed in a 20.3 cm pipe at relatively low flows. The good agreement with the LDV measurements in the viscous sub-layer provides good support for the accuracy of both techniques.

The striking aspects of the measured W_u and W_v is that they are equal at large frequencies and that differences with increasing distance from the wall are noted mainly at the low and moderate frequencies. The range of frequencies characterizing the fluctuating velocity field does not change much with wall distance, but this could be a characteristic of low Reynolds number turbulence.

There are no large ranges of frequencies where $W(n)$ varies as n^{-1} but this is to be expected for low Reynolds number flows where a log-layer does not exist. However, it is noted that an appreciable range of frequencies exists where $W_u(n)$ varies roughly as n^{-3}. This is particularly evident in the measurements made in the viscous sub-layer, shown in Fig. 15.

A similar type behavior has been observed for the spectral density function of mass transfer fluctuations at large Schmidt numbers (Sirkar and Hanratty 1970; Shaw and Hanratty 1977). Specifically Shaw and Hanratty showed that for large n that

$$\frac{\left(\frac{u^{*2}}{\nu}\right) W_k}{\bar{K}^2} = \frac{0.158 \times 10^{-3}}{n^{+3}\, Sc}. \tag{6}$$

Here W_k is the spectral density function of the mass transfer fluctuations, $\bar{K}$ is the average mass transfer coefficient and Sc is the Schmidt number.

Sirkar and Hanratty (1970) have argued that at large frequencies W_k is represented by a solution of the mass balance equation which is linear in the fluctuating quantities:

$$\frac{\partial c}{\partial t}\left[1 - \frac{U}{U_c}\right] - D\left(\frac{\partial^2 c}{\partial x^2} + \frac{\partial^2 c}{\partial y^2} + \frac{\partial^2 c}{\partial z^2}\right) = -v\frac{d\bar{C}}{dy} - u\frac{\partial \bar{C}}{\partial x}. \tag{7}$$

Here U is the local mean velocity, $\bar{C}$ is the local mean concentration, D is the diffusion coefficient and U_c is the convection velocity defined as

$$\frac{\partial}{\partial x} = -\frac{1}{U_c}\frac{\partial}{\partial t}. \tag{8}$$

According to (7) the u and v velocity fluctuations create concentration fluctuations, and therefore mass transfer fluctuations, through the terms on the right side. The concentration boundary layer is quite thin so that $d\bar{C}/dx \ll d\bar{C}/dy$ and $\partial^2 c/\partial x^2 \ll \partial^2 c/dz^2 \ll \partial^2 c/\partial y^2$. Therefore (7) can be simplified to

$$\frac{\partial c}{\partial t}\left[1 - \frac{U}{U_c}\right] - D\frac{\partial^2 c}{\partial y^2} = -v\frac{d\bar{C}}{dy}. \tag{9}$$

Sirkar and Hanratty made the further simplifying assumption that $\left[1 - \frac{U}{U_c}\right] \cong 1$ to obtain the following relation for W_k as $n \to \infty$:

$$\frac{\left(\frac{u^{*2}}{\nu}\right) W_k}{\bar{K}^2} = \frac{4\left(\frac{W_v}{y^{+4}\nu}\right)}{(2\pi n^{+3})\, Sc}. \tag{10}$$

The frequencies of the mass transfer fluctuations at large Sc are much smaller than the characteristic frequency of the velocity fluctuations so that (6) was derived for $n^+ < 10^{-2}$. In this range W_v is roughly constant and equal to $W_v(0)$. A comparison of (10) and (6) gives $W_v(0)/y^{+4}\nu = 9.8 \times 10^{-3}$.

This is larger than the value of about 4.5×10^{-3} suggested by the measurements shown in Fig. 15. A possible explanation is that errors are introduced by the assumption of $\left[1-\frac{U}{U_c}\right] \cong 1$. For example, if $\left[1-\frac{U}{U_c}\right]$ were represented by an effective average value of 0.77 one could rationalize the difference. Vassiliadou's study (1985) of convection velocities of the concentration field gives $U_c^+ \cong 5$ for $Sc = 1{,}000$. A value of $\left[1-\frac{U}{U_c}\right] = 0.77$ corresponds to $U \cong 1$. This seems reasonable since at $Sc = 1{,}000$ it corresponds to the location where the concentration is approximately equal to 0.7 of the bulk concentration.

The results obtained by Shaw and Hanratty on W_k prompted Hatziavramidis (Hatziavramidis 1978; Hanratty et al. 1977) to suggest that the high frequency part of the streamwise velocity spectrum in the viscous sub-layer is given by solution of the linear x-momentum equation. A simplified version of this, analogous to (9) is

$$\frac{\partial u}{\partial t}\left[1-\frac{U}{U_c}\right]-\nu\frac{\partial^2 u}{\partial y^2} = -v\frac{d\bar{U}}{\partial y}-\frac{1}{\varrho}\frac{\partial p}{\partial x}. \tag{11}$$

Equation (11) indicates that both $\partial p/\partial x$ and $v\ (d\bar{U}/dy)$ can cause streamwise velocity fluctuations close to the wall. Hatziavramidis (1978) argued that $\partial p/\partial x$ is important only for very high frequencies. If this is neglected and $[1-(U/U_c)]$ is approximated as unity then an analogous equation to (10) can be derived for the viscous sub-layer

$$\frac{W_u(n)}{y^{+2}} = \frac{4\,W_v(n)}{y^{+4}(2\pi n^+)^3}. \tag{12}$$

Values of $W_u(n)$ calculated from (12) using the $W_v(n)$ measurements in the viscous sub-layer are shown in Fig. 15. It is noted that the calculated $W_u(n)$ at large n are less than the measurements. Again, a possible explanation is that $[1-U/U_c]$ cannot be assumed equal to unity. For example if an effective average value of $[1-U/U_c]=0.77$ is again assumed good agreement is noted. If the convection velocity is taken as $U_c^+ = 15$ this corresponds to an effective $U = 3.5$.

Acknowledgements

This work was supported by the Office of Naval Research under Grant N00014-82K0324 administered by M. Reischman, by the National Science Foundation Grant NSF CBT 88-00980 administered by R. Wellek, and by the National Science Foundation Grant NSF ATM 86-00509 administered by R. Taylor.

References

Adrian, R. J. 1975: A bipolar, two-component laser-Doppler velocimeter. J. Phys. E4, 72–75

Adrian, R. J. 1983: Laser velocimetry. In: Fluid mechanics measurements. (ed. Goldstein, R. J.). pp. 155–244. Washington/DC: Hemisphere

Adrian, R. J.; Yao, C. S. 1987: Power spectra of fluid velocities measured by laser Doppler velocimetry. Exp. Fluids 5, 17–28

Buckles, J.; Hanratty, T. J.; Adrian, R. J. 1984: Turbulent flow over large-amplitude wavy surfaces. J. Fluid Mech. 140, 27–44

Goodwin, J. W.; Ottewill, R. H.; Pelton, R.; Vianello, G.; Yates, D. E. 1978: Control of particle size in the formation of polymer latices. Br. Polym. J. 10, 173–180

Hanratty, T. J.; Chorn, L. G.; Hatziavramidis, D. T. 1977: Turbulent fluctuations in the viscous wall region for newtonian and drag reducing fluids. Phys. Fluids 20, S112–S119

Hatziavramidis, D. T. 1978: Interpretation of the flow in the viscous wall region as a driven flow. Ph.D. thesis, University of Illinois, Urbana

Juarg, M. S.; Krieger, I. M. 1976: Emulsifier-free emulsion polymerization with ionic comonomer. J. Polym. Sci. 14, 2089–2107

Kim, J.; Moin, P.; Moser, R. 1987: Turbulence statistics in fully developed channel flow at low reynolds number. J. Fluid Mech. 177, 133–166

Lyons, S. L. 1989: A direct numerical simulation of fully developed turbulent channel flow with passive heat transfer. Ph.D. thesis, University of Illinois, Urbana

Niederschulte, M. A. 1989: Turbulent flow through a rectangular channel. Ph.D. thesis, University of Illinois, Urbana

Shaw, D. A.; Hanratty, T. J. 1977: Influence of schmidt number on the fluctuations of turbulent mass transfer to a wall. AIChE J. 23, 160–169

Sirkar, K. K.; Hanratty, T. J. 1970: Relation of turbulent mass transfer to a wall at high schmidt numbers to the velocity field. J. Fluid Mech. 44, 589–603

Vassiliadou, E. 1985: Turbulent mass transfer to a wall at large schmidt numbers. Ph.D. thesis, University of Illinois, Urbana

Received October 18, 1989